

Numerical Simulation and Analytical Modeling of Multichannel AlGaIn/GaN Devices

Quanbo He¹, Hengyu Wang¹, *Member, IEEE*, Ming Xiao¹, Yuhao Zhang¹, *Senior Member, IEEE*, Kuang Sheng¹, *Senior Member, IEEE*, and Florin Udrea

Abstract—In this article, we delve into the intricacies of carrier population and depletion in AlGaIn/GaN multichannel structures through a combination of TCAD numerical simulations and theoretical modeling. Here, we take into account the unintentional or intentional n-type doping commonly seen in experimental multichannel devices. The impact of doping and layer thickness on the carrier population in the multichannel, as well as the carrier depletion and C - V characteristics, is investigated. The simulation results demonstrate that the doping in the AlGaIn layer disrupts the balance between the 2-D electron gas (2DEG) and 2-D hole gas (2DHG), but the charge balance can be re-established with an additional pGaIn layer on top of the multichannel structure. This pGaIn layer can deplete the excessive electrons at high bias, resulting in a nearly flat electric field distribution. Moreover, an analytical model of the blocking electric field and conduction resistance in multichannel devices is built and validated by simulation. With this model, the impact of channel quantities on the device figure-of-merit (FOM) is studied and the optimization guideline of structure parameters is provided. This study provides key insights into the physics, performance space, and prospects of the multichannel gallium nitride (GaN) power devices.

Index Terms—Doped multichannel, gallium nitride (GaN), superjunction (SJ), TCAD simulations.

I. INTRODUCTION

IN RECENT years, electronic devices based on gallium nitride (GaN) have been successful in commercialization and market adoption due to the excellent material properties of GaN [1]. With wide bandgap and high electron mobility, GaN-based devices have shown significant advantages over traditional silicon-based devices, including higher breakdown

voltage, lower ON-resistance, and faster switching speeds [2], [3], [4]. One specific area of research interest within the field of GaN power devices is the development of multichannel superjunction (SJ) structures [5]. The concept of SJ, originally introduced in silicon technology, involves the formation of alternating p-type and n-type regions to achieve a high breakdown voltage and low ON-resistance simultaneously [6], [7]. Extending this concept to GaN devices creates new possibilities for enhancing their performance. In addition to conventional vertical GaN SJ [8] the lateral multichannel AlGaIn/GaN structure provides an alternative platform to realize SJ in GaN [9].

In AlGaIn/GaN structures, spontaneous and piezoelectric polarization produce the 2-D-electron-gas (2DEG) and 2-D-hole-gas (2DHG) layers [10]. The source for these carriers could be various. Studies [11], [12] suggested that electrons can be provided by the surface donor, whereas the 2DHG is not necessarily produced. On the other hand, n-type dopant or donor-like traps have also been utilized to provide 2DEG electrons. In this case, the ionized donors are usually located in the AlGaIn barrier instead of at the device surface.

For multichannel structures, the charge composition is even more complicated. In an ideal undoped multichannel, 2DEG and 2DHG are expected to form naturally, and charge balance can be achieved when they are depleted at high voltage. This leads to a natural SJ [or polarization SJ (PSJ)] as proposed by Ishida et al. [13] and [14]. Recent research [15] has also explored theoretically the channel control and parametric optimization of the PSJ. However, to date, no experimental demonstration of the ideal PSJ device has been reported. This is because, experimentally, even the unintentionally doped (UID) multichannel is likely to include donor-like traps [16], making it difficult to fulfill the natural charge balance required in PSJ.

Recently, the doped AlGaIn/GaN multichannel structure has been widely explored. A doped GaN/AlGaIn/GaN superheterojunction was theoretically proposed with n-type delta doping at the upper GaN/AlGaIn and p-type doping balance to improve the breakdown voltage (V_{BR}) [17]. Nevertheless, this structure comprising buried p-GaN layers is difficult to implement. In [18] and [19], a p-GaN structure was used as an edge termination for multichannel devices, enabling V_{BR} over 5 kV. In [20] and [21], multichannel GaN diodes and HEMTs with a P-GaN cap layer were experimentally demonstrated with V_{BR} up to 10 kV and impressive results with the specific ON-resistance dropping below the 1-D SiC limit. The acceptors in the p-GaN cap layer balance the net donor in the multichannel when the device is depleted, producing uniform electric field distribution.

Manuscript received 23 October 2023; revised 31 December 2023; accepted 24 January 2024. Date of publication 15 February 2024; date of current version 1 March 2024. The review of this article was arranged by Editor S. Warnock. (Corresponding authors: Florin Udrea; Hengyu Wang.)

Quanbo He and Florin Udrea are with the Department of Engineering, University of Cambridge, CB2 1TN Cambridge, U.K. (e-mail: qh243@cam.ac.uk; fu10000@cam.ac.uk).

Hengyu Wang is with the Department of Engineering, University of Cambridge, CB2 1TN Cambridge, U.K., and also with the College of Electrical Engineering, Zhejiang University, Hangzhou 310058, China (e-mail: wanghengyu@zju.edu.cn).

Ming Xiao and Yuhao Zhang are with the Center of Power Electronics Systems, Virginia Polytechnic Institute and State University, Blacksburg, VA 24060 USA (e-mail: yhzhang@vt.edu).

Kuang Sheng is with the College of Electrical Engineering, Zhejiang University, Hangzhou 310027, China.

Color versions of one or more figures in this article are available at <https://doi.org/10.1109/TED.2024.3359165>.

Digital Object Identifier 10.1109/TED.2024.3359165

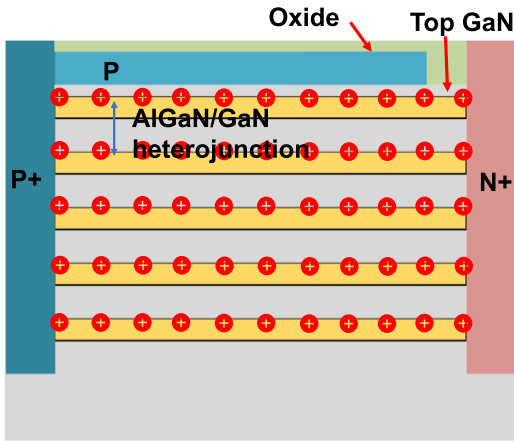


Fig. 1. Schematic of the five-channel AlGaIn/GaN heterojunction PSJ device with long p-type GaN cap.

This article delves into the behavior of carriers and their depletion in a doped GaN multichannel structure, featuring a P-GaN cap layer. We achieve this insight through TCAD simulations and analytical modeling. Our core aim is to uncover the physics behind carrier generation and depletion in both doped and natural multichannel GaN SJ structures. In addition, we work toward enhancing the lateral SJ figure-of-merit (FOM) by optimizing channel quantities. It is important to highlight that our study solely concentrates on electrical simulation and model analysis, with no consideration for thermal impact or hot electron effects.

II. SIMULATION STUDY

A. Simulation Setup and Calibration

In this study, a charge balance heterostructure device is employed to analyze the formation and depletion of 2DEG and 2DHG, as shown in Fig. 1. Compared to experimental devices [20], [21], this structure simplifies the edge termination and is applicable to both diodes and transistors. Anode and cathode are on each side, both with ohmic contact. The structure comprises five channels and a GaN buffer layer. The length of pGaIn layer is designed as $40\ \mu\text{m}$. AlGaIn layers contain n-type dopants to balance the charge with the top p-type GaN. The product of donor concentration and doping thickness in all five AlGaIn barriers is equal to the product of N_A and thickness of pGaIn. The Al mole fraction is 0.25. In order to investigate the depletion behavior of 2DEG and 2DHG, a very thin GaN undoped cap is added. In the case of undoped AlGaIn, equal concentrations of mobile 2DHG and 2DEG are derived from matching polarized charge conversions [15].

The simulation calibration was based on the experimental device reported in [21], in which a five-channel diode with a 120-nm pGaIn cap was fabricated. The [Mg] concentration in the p-GaN is $4 \times 10^{18}\ \text{cm}^{-3}$. As previously reported in [22], the MOCVD-grown pGaIn typically exhibits a near 100% ratio between [Mg] and the acceptor concentration after activation when [Mg] is in the low $10^{18}\ \text{cm}^{-3}$ range. Hence, in our simulation, we set N_A to be also $4 \times 10^{18}\ \text{cm}^{-3}$. The multichannel is UID but contains net donors, which contribute to 2DEG together with the polarization charges. The experimental $C-V$ characteristics reflect the successive charge depletion in different channels.

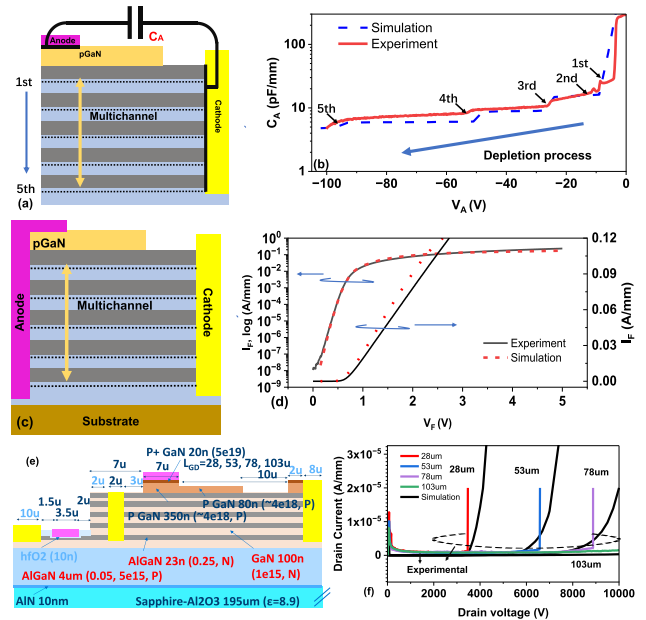


Fig. 2. (a) Schematic of the CV test structure. (b) Experimental and simulated $C-V$ curves for a five-channel structure with pGaIn cap. (c) Schematics of the multichannel AlGaIn/GaN SBD. (d) Experimental and simulated forward $I-V$ characteristics of SBD. (e) Two-dimensional cross section of the AlGaIn/GaN MC²-HEMT device. (f) Experimental, simulated, and model OFF-state $I-V$ curves of E-mode MC²-HEMTs with different L_{GD}^{MC} . The 103- μm device did not breakdown at experimental test limits.

A number of specific models were used to determine the electrical characteristics. For instance, piezoelectric polarization and strain models are significant to simulate the polarization effects arising between AlGaIn/GaN heterojunctions. Mobility models are specified to describe the carrier mobility, including high-field saturation effects. Effective intrinsic density and Fermi-level models are included. A Shockley-Read-Hall (SRH) model is used to characterize recombination through deep defect levels in the gap [23].

In TCAD simulations, the Poisson equation is solved before the coupled equations for electrons and holes. This ensures that the electric potential distribution is determined, before treating for carrier transport. Meanwhile, important quantities, such as electric field and current flow, can be calculated.

With this setup, the simulated $C-V$ characteristics agree with experimental results [Fig. 2(b)], illustrating the $C-V$ characteristics under progressively higher reverse biases. The curve demonstrates the complete depletion of the multichannel structure, as evidenced by the clear delineation of steps corresponding to each individual channel. To further validate the carrier profile and transport models in the simulation, we calibrate the simulation with the forward current-voltage ($I-V$) characteristics of the multichannel Schottky barrier diode (SBD) reported in [20]. The structure of this multichannel SBD is shown in Fig. 2(c), and its only difference from the $C-V$ diode structure in Fig. 2(a) is an additional Schottky contact to five channels. Fig. 2(d) shows the simulated and experimental forward $I-V$ characteristics. The good agreement further validates our simulation models. Furthermore, the simulation model is also calibrated with the multichannel monolithic-cascode HEMT (MC²-HEMT) from [21]. Fig. 2(e) illustrates the 2-D cross section of the MC²-HEMT structure and Fig. 2(f) shows the agreement of OFF-state $I-V$ curves

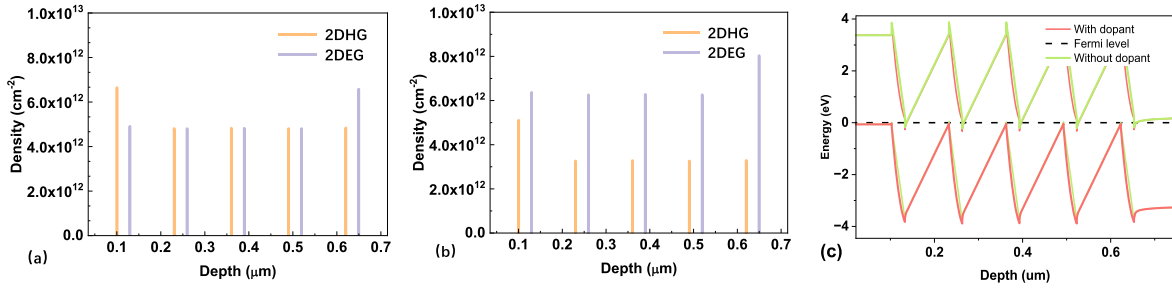


Fig. 3. (a) Carrier distribution in five channels without n-type dopant in AlGaIn barrier. (b) Carrier distribution in five channels with n-type dopant in AlGaIn barriers. (c) Energy band at zero bias with and without n-type dopant in AlGaIn barrier.

with different gate–drain distances (L_{GD}^{MC}) between experimental and simulated ones.

B. Impact of n-Type Doping on Carrier Density

Fig. 3(a) shows the distribution of carriers in a five-channel diode with an undoped AlGaIn barrier. The 2DEG concentration in the top and middle channels is almost identical, while the 2DEG concentration in the bottom channel is substantially higher, due to the absence of back barrier. 2DHG in the middle and bottom channels is also almost the same, while the 2DHG in the top channel is higher, which ensures the charge balance.

Fig. 3(b) illustrates the carrier distribution in a five-channel diode with a doping concentration of $2.7 \times 10^{18} \text{ cm}^{-3}$ in each AlGaIn barrier. At this concentration, the balance between the 2DHG and the 2DEG has been disrupted. The presence of n-type dopants provides an additional source for 2DEG and depletes 2DHG simultaneously. The 2DEG density is increased, while the 2DHG density is decreased. The energy band in Fig. 3(c) illustrates the electron and hole wells visually. Note that the increase in 2DEG density is lower than the charge density from the donors in the multichannel. In this structure, the holes supplied by the pGaIn cap balance with excess electrons in the multichannel.

C. Impact of Layers Thickness on Carrier Density

In addition to the effects of the AlGaIn barrier doping, the electron concentration in these channels also relies on both the thickness of the AlGaIn barrier and the GaIn channel. At this point, the concentration of electrons and holes in the channel is determined by the thickness of AlGaIn and GaIn, as shown in Figs. 4 and 5.

According to the simulation results of the undoped device, Figs. 4(a) and (b) and 5(a) and (b), the net carrier charge is zero, while the increase of t_{AlGaIn} and t_{GaIn} will increase the carrier density at each channel. Furthermore, for different t_{AlGaIn} and t_{GaIn} , the simulation shows that the electron and hole distribution in each channel still follows the pattern, that the top-hole gas and bottom electron gas densities are always higher than in the middle channel and that the amount of excess top 2DHG and bottom 2DEG is almost the same. In this case, the electron concentration ($N_{s,\text{mid}}$) is equal to the hole concentration ($P_{s,\text{mid}}$) in middle channels, while the top channel hole concentration ($P_{s,\text{top}}$) balance is to the bottom of electron concentration ($N_{s,\text{top}}$) [15]. However, it is important to note that excessively thin barrier thickness, specifically AlGaIn layers below 10 nm, leads to diminished polarization effects, thereby impeding the proper 2DEG generation.

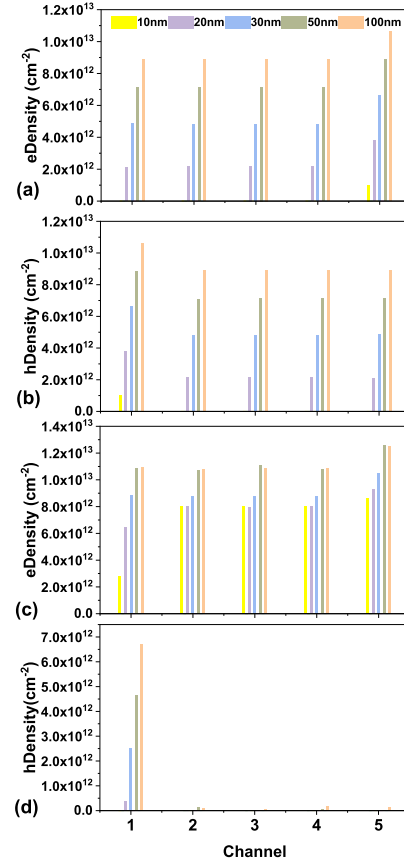


Fig. 4. (a) Electron and (b) Hole distribution in five channels (from top to bottom) for different AlGaIn thicknesses when the device is undoped. (c) Electron and (d) hole distribution in five channels (from top to bottom) for different AlGaIn thicknesses when AlGaIn is n-type doped, the device is in charge balance. All GaIn barrier thicknesses are kept at 100 nm.

Figs. 4(c) and (d) and 5(c) and (d) illustrate the carrier density in the doped device. In these structures, the whole carrier keeps a charge balance. Like their undoped counterparts, the carrier concentrations in the doped devices also experience enhancement, with an increase in the AlGaIn and GaIn thickness; however, the magnitude of change is relatively less pronounced than that observed in undoped situations. Moreover, the hole concentration in the last four channels is negligible because of the n-type doping. Since most of the doped carriers have been derived from impurities and the thickness can only influence the polarization, the effect of the change in the thickness of the doped potential barrier on the carrier concentration is not as prominent as it is in the undoped case, in comparison.

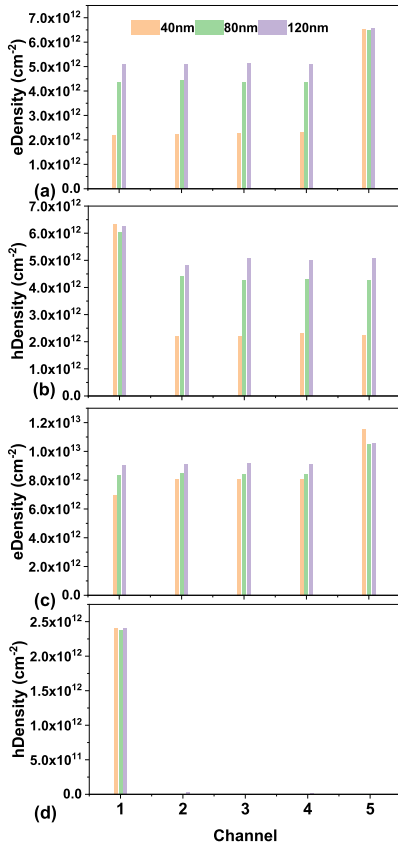


Fig. 5. (a) Electron and (b) hole distribution in five channels (from top to bottom) for different GaN thicknesses when the device is undoped. (c) Electron and (d) hole distribution in five channels (from top to bottom) for different GaN thicknesses when AlGaN is n-type doped, the device is in charge balance. All AlGaN barrier thicknesses are kept at 30 nm.

D. Impact of n-Type Doping on Channel Carrier Depletion

As shown in Fig. 6(a), in the present simulation model, when AlGaN barriers are undoped, the depletion of the uppermost four 2DEG channels happens simultaneously, while the lowermost 2DEG channel persists without depletion until exposed to elevated voltages due to its high density. Note that when the polarization charge is very high, the middle channel electrons may not be fully depleted at the same time. However, when the AlGaN layer is doped, the depletion of the 2DEG channels takes place sequentially, as shown in Fig. 6(b). In the simulation model, specifically in the reverse bias process, the depletion occurs in a sequential manner, progressing from the upper channel to the lower ones. Nevertheless, during the depletion of the upper channel, a small reduction in the charge in the adjacent lower channel is observed. Meanwhile, depletion of the upper channel leads to a small reduction of carriers in the lower channel. Initially, the holes and electrons deplete each other, leading to a gradual reduction in carrier density. Subsequently, the excess electron in the multichannel needs to be depleted from top to bottom by the pGaN cap layer. Consequently, over 400 V of bias is required to achieve full depletion, as shown in Fig. 6(b).

E. Impact of Layer Thickness on C–V Characteristics

The effect of AlGaN and GaN layers thickness on electron and hole concentration, as well as the depletion rate,

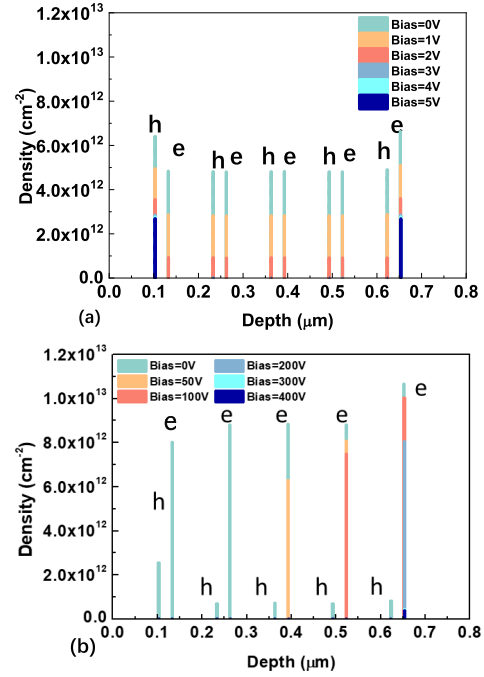


Fig. 6. (a) Electron and hole depletion in each layer at different bias voltages in the undoped case of the device (cut at $L_{ac} = 2 \mu\text{m}$). (b) Electron and hole depletion in each layer at different bias voltages in the doped case of the device (cut at $L_{ac} = 2 \mu\text{m}$).

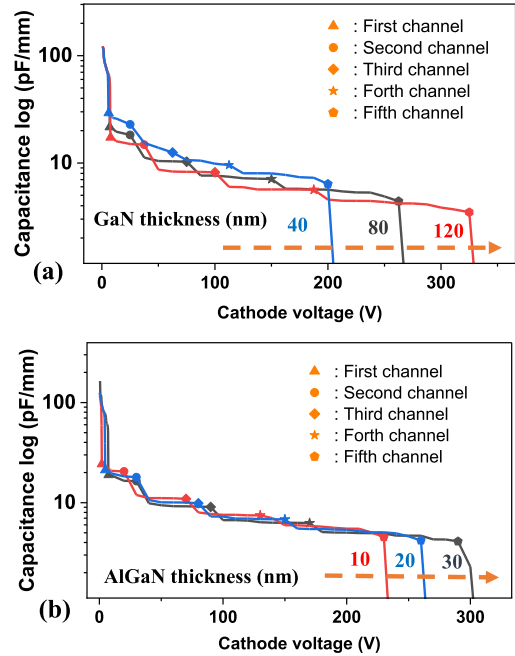


Fig. 7. (a) C–V characteristics for different GaN thicknesses when the AlGaN barrier is 30 nm and with n-type dopant, the device is in charge balance. (b) C–V characteristics for different AlGaN thicknesses when the GaN barrier is 100 nm, and with n-type dopant, the device is in charge balance.

was examined for various layer thicknesses. Further analysis using C–V characterization reveals distinct differences in the capacitance behavior for different GaN and AlGaN layers' thicknesses, as shown in Fig. 7.

The results in Fig. 7 show that at zero bias, the capacitance of device with a thin layer GaN or AlGaN is substantially higher than that of devices with a thick layer, which is

consistent to the basic capacitance equation where the value of capacitance is inversely proportional to the distance of two electrode plates. As the bias on the device gradually increases, the electrons and holes in the channels start to be depleted. For the n-type-doped multichannel structure, excess electrons in each channel must be depleted by the top P-GaN layer, as holes in channels are quickly depleted below 1 V. Therefore, for device with a thin GaN layer, the sequential depletion of the five channels is faster than that of the device with a thick GaN layer. Furthermore, the 5th channel requires a bias voltage of >200 V to begin depletion and higher voltages are required for complete depletion. It is interesting to note that the voltage required for channel depletion is lower for the device with the thinner GaN or AlGaIn layer when compared to the device with the thicker layer. This result is due to the stronger capacitive coupling of the top P-GaN layer and the 2DEGs.

F. Electric Field Distribution in Charge Balance Structure

The investigation of electric field distribution is of paramount importance in the study of power devices [24]. In this study, we have focused on the electric field distribution in the OFFstate of the device with the balanced charge. In the undoped multichannel structures, one characteristic feature is the presence of a flat electric field profile along the entire drift region. This phenomenon arises from the quick carrier depletion, which occurs at a remarkably low voltage (V_{cathode}) across the drift region, as discussed in Section II-D. On the other hand, when the AlGaIn layers are doped, although there are excessive electrons that cannot be fully depleted by 2DHGs, the pGaN top layer facilitates the depletion. As a result, the vertical depletion is achieved within several hundred volts and the electric field peak in the drift region is kept low. Due to the charge balance effect, the large portion of the drift region has a uniform flat electric field. Therefore, these multichannel devices are enabled to attain exceptionally high V_{BR} values. The 2-D electric field distribution is shown in Fig. 8(a)–(d) and the cutline along the drift region, at various bias voltages, is shown in Fig. 8(e). It should be noted that edge effects introduce a slight increase in the electric field on both anode and cathode sides.

III. ANALYTICAL MODEL OF GAN MULTICHANNEL STRUCTURE

A vertical asymmetrical n-type doping structure with multiple channels is considered in model [Fig. 9]. The net charge in the AlGaIn/GaN structure is produced by the ionized donors and only exists in AlGaIn. The electric field is distributed in a discontinuous form, due to the interface charge.

The electric field distribution can be derived from Poisson's equation and Gaussian law. An approximation of linear electric field distribution is used [6] and the electric field in the x - and y -directions is built separately. In the y -direction, the electric field in the n th GaN ($E_{\text{GaN}-yn}$) and AlGaIn ($E_{\text{AlGaIn}-yn}$) barrier can be expressed using the following equations:

$$E_{\text{GaN}-yn} = \frac{q \cdot N_{\text{AlGaIn}} \cdot t_{\text{AlGaIn}}}{\epsilon} \quad (1)$$

$$\frac{dE_{\text{AlGaIn}-n}}{dy} = \frac{q \cdot N_{\text{AlGaIn}}}{\epsilon} \quad (2)$$

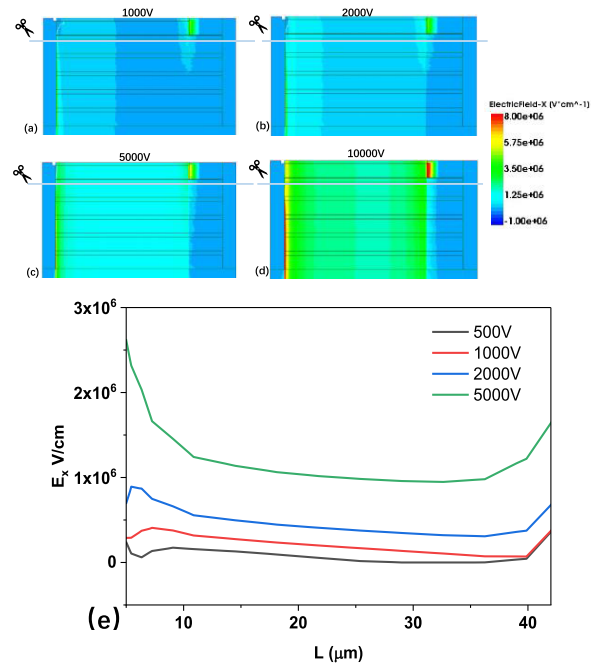


Fig. 8. (a)–(d) X-direction electric field contour for different V_D (with AlGaIn doping). (e) X-direction electric field in profile at the bottom AlGaIn/GaN interface of the device for different V_D (with AlGaIn doping).

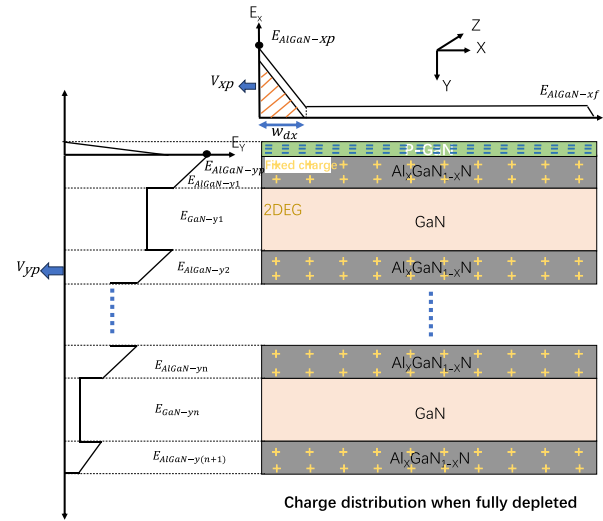


Fig. 9. Vertical asymmetrical n-type doping model with n channels and theoretical electric field.

where q is the electron charge, N_{AlGaIn} is the doping concentration of AlGaIn barrier, and t_{AlGaIn} is the AlGaIn barrier thickness. Because the permittivity of AlGaIn and GaN is close, ϵ is used to present that of those two materials. In the multichannel device model, the vertical electric field is distributed as a stepped pattern from top to bottom, as shown in Fig. 9.

In the x -direction, the following equation represents the electric field distribution in the AlGaIn barrier:

$$\frac{E_{\text{AlGaIn}-xp} - E_{\text{AlGaIn}-xf}}{w_{dx}} = \frac{q \cdot N_{\text{AlGaIn}}}{\epsilon} \quad (3)$$

where $E_{\text{AlGaIn}-xp}$ is the peak electric field in the x -direction, $E_{\text{AlGaIn}-xf}$ is the flat electric field of x -direction, and w_{dx} is the depletion width in the x -direction at the condition when

the vertical depletion is completed. We approximate the peak voltage of the x -direction as the product of the flat electric field ($E_{\text{AlGaN-}xf}$) and the x -length (L_x). At the point

$$(E_c^2 - E_{\text{AlGaN-}y1}^2) = E_{\text{AlGaN-}xp}^2 \approx E_c^2 \quad (4)$$

where E_c is the critical electric field when the breakdown occurs. In this equation, as $E_{\text{AlGaN-}y1}$ is significantly smaller than $E_{\text{AlGaN-}xp}$ at high voltage, the impact of $E_{\text{AlGaN-}y1}$ can be ignored and the breakdown voltage is dominated by $E_{\text{AlGaN-}xp}$

$$\begin{aligned} E_{\text{AlGaN-}xf} &= E_{\text{AlGaN-}xp} - \frac{q \cdot N_{\text{AlGaN}}}{\epsilon} * w_{dx} \\ &= E_c - \frac{q \cdot N_{\text{AlGaN}}}{\epsilon} * w_{dx} \end{aligned} \quad (5)$$

w_{dx} can be derived from

$$V_{xp} = \frac{1}{2} \frac{q \cdot N_{\text{AlGaN}}}{\epsilon} * w_{dx}^2. \quad (6)$$

Because of the simultaneous depletion from both x - and y -directions in the beginning, a potential drop peak in the x -direction (V_{xp}) is equal to the potential drop peak in the y -direction (V_{yp}). The potential drop in the y -direction is

$$\begin{aligned} V_{yp} &= \frac{n \cdot q \cdot N_{\text{AlGaN}} \cdot t_{\text{AlGaN}}}{2\epsilon} \cdot [n \cdot t_{\text{AlGaN}} + (n-1)t_{\text{GaN}}] \\ &\quad + \Delta E_p \cdot n \cdot t_{\text{AlGaN}} + \frac{q \cdot N_{\text{pGaN}} \cdot t_{\text{pGaN}}^2}{2\epsilon} \end{aligned} \quad (7)$$

where t_{AlGaN} is the thickness of GaN barrier and ΔE_p is an abrupt electric field change due to a polarization field and is a constant. N_{pGaN} is the doping concentration of pGaN and t_{pGaN} is the pGaN thickness. By substituting (6) and (7) into (5), V_{BR} can be expressed as (8), shown at the bottom of the page. Note that this requires E_{yp} smaller than E_c . When E_{yp} is equal to E_c , vertical breakdown occurs. At this point, the magnitude of V_{BR} can be considered close to V_{yp} . At high doping concentration, a greater number of channels is more likely to cause vertical breakdown.

Fig. 10 shows the simulated and modeled values in the Y -direction in the zero-bias state. In the doped structure, the ionized electrons from the AlGaN doping are swept into the nearby quantum well (QW), resulting in a slope of the electric field distribution in AlGaN, as shown in Fig. 10(b). The net surface charge is calculated by summing up the polarization charge, electron density, and hole density. Furthermore, we determine the relationship between the electric fields at the top and bottom channels.

The equations indicate that AlGaN doping concentration, AlGaN, and GaN thickness play significant roles in multichannel devices. The model can also be verified by calibrating with experimental results in Fig. 11.

IV. PREDICTION AND DISCUSSION

Multichannel structures have long been utilized in power devices to reduce specific ON-resistance ($R_{\text{ON,sp}}$) [18], [25],

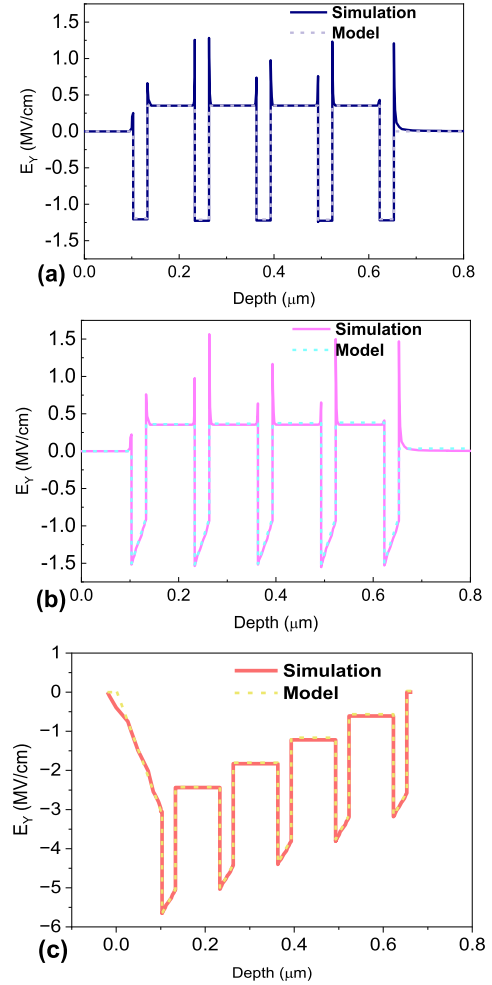


Fig. 10. (a) Y -direction simulation and model of the electric field without dopant. (b) Y -direction simulation of the electric field with AlGaN barriers n -type dopant. (c) Y -direction simulation of the electric field with AlGaN barriers n -type dopant when 2DEG is depleted at high voltage.

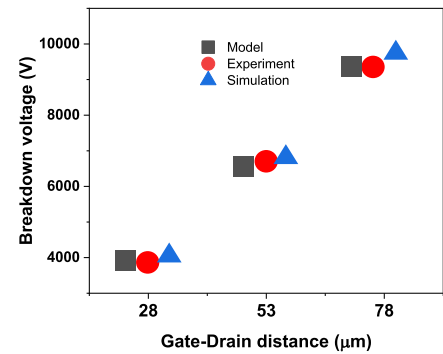


Fig. 11. Model, experimental, and simulation V_{BR} of E -mode MC2-HEMTs with different L_{GD}^{MC} . Breakdown voltage is extracted at leakage current density = 2×10^{-5} A/mm.

[26], [27]. The tradeoff between $R_{\text{ON,sp}}$ and V_{BR} for natural SJ structures is discussed in [5], but there is no such analysis

$$V_{BR} = E_{\text{AlGaN-}xf} \cdot L_x = \left[E_c - \frac{q \cdot N_{\text{AlGaN}}}{\epsilon} \cdot \sqrt{\frac{n \cdot t_{\text{AlGaN}} \cdot [n \cdot t_{\text{AlGaN}} + (n-1)t_{\text{GaN}} + 2\epsilon \Delta E_p / q N_{\text{AlGaN}}]}{+ N_{\text{pGaN}} t_{\text{pGaN}}^2 / N_{\text{AlGaN}}}} \right] L_x \quad (8)$$

available for doped SJ configurations. The advantage of multi-channel devices lies in their ability to increase the cumulative 2DEG, thus reducing the ON-resistance while maintaining a favorable breakdown ability. Therefore, increasing the number of channels has been considered. In this model, the quantity of channels is defined as a variable parameter. The analytical model expresses the specific ON-resistance as

$$R_{ON,sp} \approx \frac{L_x^2}{n \cdot q \cdot N_s \cdot \mu} \quad (9)$$

where L_x is the length in the x -direction, N_s refers electron concentration, μ refers electron mobility, n represents channel quantities, and w is the channel width.

However, it should be noted that the number of channels cannot be increased indefinitely, due to limitations imposed by various parameters. To investigate the impact on channel properties, we assume a constant mobility of $1930 \text{ cm}^2 \cdot \text{V}^{-1} \cdot \text{s}^{-1}$. Based on these parameters, the FOM of lateral SJ can be expressed as (10), shown at the bottom of the page, where E_c is the electric field, N_{AlGaN} is the doping concentration of AlGaN barrier, and ε is the permittivity. Several key parameters, including the AlGaN thickness, doping concentration, channel number, electron concentration, and mobility, play significant roles in influencing the FOM. In simple terms, N_s can be viewed as consisting of a combination of dopant ionization and polarization charges. As the doping concentration and the thickness of barriers vary, the values of the dopant ionization (assuming a fully ionized) and the polarization charges also change. Considering the results' accuracy, the model was integrated with simulations, and the values of N_s under various parameters were extracted from these simulations. Channel quantity, AlGaN barrier doping concentration, and GaN layer thickness are defined as variable parameters. To keep the model accurate, the value within the square in (10) must be positive, which is

$$\sqrt{\frac{n \cdot t_{\text{AlGaN}} \cdot [n \cdot t_{\text{AlGaN}} + (n-1)t_{\text{GaN}} + 2\varepsilon \Delta E_p / q N_{\text{AlGaN}}] + N_{\text{pGaN}} t_{\text{pGaN}}^2 / N_{\text{AlGaN}}}{N_{\text{AlGaN}}}} \quad (11)$$

To analyze the impact of AlGaN barrier doping concentration, the thickness of the AlGaN and GaN layers is kept constant at 20 nm. In Fig. 12(a), the role of AlGaN doping concentration becomes evident. Theoretically, in the case of high dopant concentration, a larger number of channels results in smaller FOM values. When considering only the thickness of GaN as a variable parameter ($N_{\text{AlGaN}} = 1 \times 10^{18} \text{ cm}^{-3}$), the effect of GaN thickness is not significant, but the effect of the number of channels on FOM is more pronounced, as illustrated in Fig. 12(b). Similarly, when considering only the thickness of AlGaN as a variable parameter, a thinner AlGaN layer corresponds to higher FOM values when n is more than 4, as illustrated in Fig. 11(c). However, it is worth noting that an

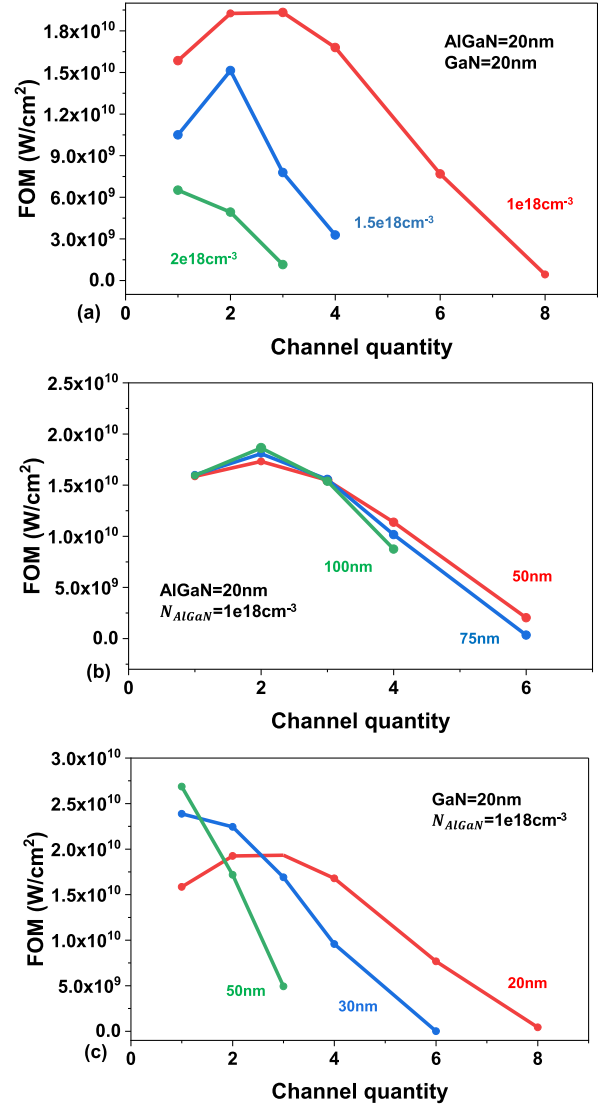


Fig. 12. (a) FOM plotted with channel quantities at different AlGaN layer doping concentrations. (b) FOM plotted with channel quantities at different GaN layer thicknesses. (c) FOM plotted with channel quantities at different AlGaN layer thicknesses.

excessively large number of channels is not realistic in practical applications and poses significant fabrication challenges and a smaller number of channels increase resistance. Hence, a tradeoff is needed.

A higher FOM value indicates a more desirable power device with better performance. However, it should be noted that FOM alone does not reflect all aspects of device performance. Other factors, such as thermal considerations, switching speed, and reliability, should also be considered when selecting a power semiconductor device for a specific application. Considering the tradeoff between manufacturing challenges and FOM, when AlGaN and GaN thicknesses are

$$\text{FOM} = \frac{V_{BR}^2}{R_{ON,sp}} \approx q \cdot N_s \cdot \mu \cdot n \cdot \left\{ E_c - \frac{q \cdot N_{\text{AlGaN}}}{\varepsilon} \sqrt{\frac{n \cdot t_{\text{AlGaN}} \cdot [n \cdot t_{\text{AlGaN}} + (n-1)t_{\text{GaN}} + 2\varepsilon \Delta E_p / q N_{\text{AlGaN}}] + N_{\text{pGaN}} t_{\text{pGaN}}^2 / N_{\text{AlGaN}}}{N_{\text{AlGaN}}}} \right\}^2 \quad (10)$$

lower than 50 and 100 nm, respectively, channel quantities of around 4 or 5 are the most appropriate.

V. CONCLUSION

In conclusion, this article investigates the intricacies of channel control and carrier generation in the GaN-based doped multichannel SJ structures. By employing a theoretical model and conducting TCAD Sentaurus simulations, the behavior of these devices has been thoroughly analyzed.

The research reveals that the net charge in the AlGaIn/GaN structure is usually produced by ionized donor states and exists mainly in the AlGaIn layer. Such doping disrupts the balance between the hole and electron carriers, increasing 2DEG and suppressing 2DHG. Simulation results further demonstrate that the carrier concentration in each channel is influenced by the thickness of the AlGaIn barrier and the GaN channel. The depletion behavior of 2DEG and 2DHG in undoped and doped multichannel structures are analyzed, revealing sequential depletion in doped structures and simultaneous depletion in undoped structures.

The presence of a p-type GaN cap layer is essential to balance the depletion charges. In undoped structures, the electric field profile is flat along the entire drift region, while in doped structures, higher voltages are required for carrier depletion. The presence of a pGaIn layer helps maintain a flat electric field profile, allowing these multichannel devices to achieve high V_{BR} .

Based on the analysis and simulation results, the carrier concentration is influenced by the thickness of the barriers and the doping concentration. Thicker barriers and higher doping levels lead to increased N_s . This impact extends to the FOM. In the context of multichannel structures, having more channels results in a greater 2DEG. Nevertheless, considering the tradeoff between $R_{ON,SP}$ and V_{BR} , a higher N_s does not necessarily equate to better performance. An increment in the number of channels generally leads to an increase in the FOM across various parameters. However, pushing the channel count even higher tends to result in a subsequent decrease in the FOM. For a common situation, AlGaIn barrier thicknesses of 30 nm (with doping concentrations approximately $1 \times 10^{18} \text{ cm}^{-3}$) and GaN barrier thicknesses of 100 nm, it is advisable to limit the number of channels to approximately 4–5 for the more commonly used structures.

REFERENCES

- [1] J. P. Kozak et al., "Stability, reliability, and robustness of GaN power devices: A review," *IEEE Trans. Power Electron.*, vol. 38, no. 7, pp. 8442–8471, Jul. 2023, doi: [10.1109/TPEL.2023.3266365](https://doi.org/10.1109/TPEL.2023.3266365).
- [2] M. Meneghini et al., "GaN-based power devices: Physics, reliability, and perspectives," *J. Appl. Phys.*, vol. 130, no. 18, Nov. 2021, Art. no. 181101, doi: [10.1063/5.0061354](https://doi.org/10.1063/5.0061354).
- [3] F. Roccaforte et al., "Emerging trends in wide band gap semiconductors (SiC and GaN) technology for power devices," *Microelectronic Eng.*, vols. 187–188, pp. 66–77, Feb. 2018, doi: [10.1016/j.mee.2017.11.021](https://doi.org/10.1016/j.mee.2017.11.021).
- [4] U. K. Mishra, P. Parikh, and Y.-F. Wu, "AlGaIn/GaN HEMTs—An overview of device operation and applications," *Proc. IEEE*, vol. 90, no. 6, pp. 1022–1031, Jun. 2002, doi: [10.1109/JPROC.2002.1021567](https://doi.org/10.1109/JPROC.2002.1021567).
- [5] Y. Zhang, F. Udrea, and H. Wang, "Multidimensional device architectures for efficient power electronics," *Nature Electron.*, vol. 5, no. 11, pp. 723–734, Nov. 2022, doi: [10.1038/s41928-022-00860-5](https://doi.org/10.1038/s41928-022-00860-5).
- [6] T. Fujihira, "Theory of semiconductor superjunction devices," *Jpn. J. Appl. Phys.*, vol. 36, no. 10, p. 6254, Oct. 1997, doi: [10.1143/jjap.36.6254](https://doi.org/10.1143/jjap.36.6254).
- [7] F. Udrea, G. Deboy, and T. Fujihira, "Superjunction power devices, history, development, and future prospects," *IEEE Trans. Electron Devices*, vol. 64, no. 3, pp. 713–727, Mar. 2017, doi: [10.1109/TED.2017.2658344](https://doi.org/10.1109/TED.2017.2658344).
- [8] M. Xiao et al., "First demonstration of vertical superjunction diode in GaN," in *IEDM Tech. Dig.*, Dec. 2022, p. 35, doi: [10.1109/IEDM45625.2022.10019405](https://doi.org/10.1109/IEDM45625.2022.10019405).
- [9] L. Nela, M. Xiao, Y. Zhang, and E. Matioli, "A perspective on multi-channel technology for the next-generation of GaN power devices," *Appl. Phys. Lett.*, vol. 120, no. 19, May 2022, Art. no. 190501, doi: [10.1063/5.0086978](https://doi.org/10.1063/5.0086978).
- [10] O. Ambacher et al., "Two-dimensional electron gases induced by spontaneous and piezoelectric polarization charges in N- and Ga-face AlGaIn/GaN heterostructures," *J. Appl. Phys.*, vol. 85, no. 6, pp. 3222–3233, Mar. 1999, doi: [10.1063/1.369664](https://doi.org/10.1063/1.369664).
- [11] J. P. Ibbetson, P. T. Fini, K. D. Ness, S. P. DenBaars, J. S. Speck, and U. K. Mishra, "Polarization effects, surface states, and the source of electrons in AlGaIn/GaN heterostructure field effect transistors," *Appl. Phys. Lett.*, vol. 77, no. 2, pp. 250–252, Nov. 2000, doi: [10.1063/1.126940](https://doi.org/10.1063/1.126940).
- [12] S. Heikman, S. Keller, Y. Wu, J. S. Speck, S. P. DenBaars, and U. K. Mishra, "Polarization effects in AlGaIn/GaN and GaN/AlGaIn/GaN heterostructures," *J. Appl. Phys.*, vol. 93, no. 12, pp. 10114–10118, Jun. 2003, doi: [10.1063/1.1577222](https://doi.org/10.1063/1.1577222).
- [13] H. Ishida et al., "Unlimited high breakdown voltage by natural super junction of polarized semiconductor," *IEEE Electron Device Lett.*, vol. 29, no. 10, pp. 1087–1089, Oct. 2008, doi: [10.1109/LED.2008.2002753](https://doi.org/10.1109/LED.2008.2002753).
- [14] H. Ishida et al., "GaN-based natural super junction diodes with multi-channel structures," in *IEDM Tech. Dig.*, San Francisco, CA, USA, Dec. 2008, pp. 1–4, doi: [10.1109/IEDM.2008.4796636](https://doi.org/10.1109/IEDM.2008.4796636).
- [15] L. Nela, C. Erine, A. M. Zadeh, and E. Matioli, "Intrinsic polarization super junctions: Design of single and multichannel GaN structures," *IEEE Trans. Electron Devices*, vol. 69, no. 4, pp. 1798–1804, Apr. 2022, doi: [10.1109/TED.2022.3151558](https://doi.org/10.1109/TED.2022.3151558).
- [16] R. Lingaparthi, N. Dharmarasu, K. Radhakrishnan, A. Ranjan, T. L. A. Seah, and L. Huo, "Source of two-dimensional electron gas in unintentionally doped AlGaIn/GaN multichannel high-electron-mobility transistor heterostructures," *Appl. Phys. Lett.*, vol. 118, no. 12, Mar. 2021, Art. no. 122105, doi: [10.1063/5.0045910](https://doi.org/10.1063/5.0045910).
- [17] S.-W. Han, J. Song, and R. Chu, "Design of GaN/AlGaIn/GaN super-heterojunction Schottky diode," *IEEE Trans. Electron Devices*, vol. 67, no. 1, pp. 69–74, Jan. 2020, doi: [10.1109/TED.2019.2953843](https://doi.org/10.1109/TED.2019.2953843).
- [18] M. Xiao et al., "3.3 kV multi-channel AlGaIn/GaN Schottky barrier diodes with P-GaN termination," *IEEE Electron Device Lett.*, vol. 41, no. 8, pp. 1177–1180, Aug. 2020, doi: [10.1109/LED.2020.3005934](https://doi.org/10.1109/LED.2020.3005934).
- [19] M. Xiao et al., "5 kV multi-channel AlGaIn/GaN power Schottky barrier diodes with junction-fin-anode," in *IEDM Tech. Dig.*, San Francisco, CA, USA, Dec. 2020, pp. 1–4, doi: [10.1109/IEDM13553.2020.9372025](https://doi.org/10.1109/IEDM13553.2020.9372025).
- [20] M. Xiao, Y. Ma, K. Liu, K. Cheng, and Y. Zhang, "10 kV, 39 mΩ-cm² multi-channel AlGaIn/GaN Schottky barrier diodes," *IEEE Electron Device Lett.*, vol. 42, no. 6, pp. 808–811, Jun. 2021, doi: [10.1109/LED.2021.3076802](https://doi.org/10.1109/LED.2021.3076802).
- [21] M. Xiao et al., "Multi-channel monolithic-cascade HEMT (MC2-HEMT): A new GaN power switch up to 10 kV," in *IEDM Tech. Dig.*, San Francisco, CA, USA, Dec. 2021, pp. 1–4, doi: [10.1109/IEDM19574.2021.9720714](https://doi.org/10.1109/IEDM19574.2021.9720714).
- [22] A. Castiglia, J.-F. Carlin, and N. Grandjean, "Role of stable and metastable Mg–H complexes in p-type GaN for CW blue laser diodes," *Appl. Phys. Lett.*, vol. 98, no. 21, May 2011, Art. no. 213505, doi: [10.1063/1.3593964](https://doi.org/10.1063/1.3593964).
- [23] *Sentaurus™ Device User Guide*, Synopsys, Mountain View, CA, USA, 2015.
- [24] G. Meneghesso, M. Meneghini, and E. Zanoni, "Breakdown mechanisms in AlGaIn/GaN HEMTs: An overview," *Jpn. J. Appl. Phys.*, vol. 53, no. 10, Oct. 2014, Art. no. 100211, doi: [10.7567/jjap.53.100211](https://doi.org/10.7567/jjap.53.100211).
- [25] J. Ma, G. Kampitsis, P. Xiang, K. Cheng, and E. Matioli, "Multi-channel tri-gate GaN power Schottky diodes with low ON-resistance," *IEEE Electron Device Lett.*, vol. 40, no. 2, pp. 275–278, Feb. 2019, doi: [10.1109/LED.2018.2887199](https://doi.org/10.1109/LED.2018.2887199).
- [26] J. Ma et al., "1200 V multi-channel power devices with 2.8Ω-mm ON-resistance," in *IEDM Tech. Dig.*, San Francisco, CA, USA, Dec. 2019, p. 1–4, doi: [10.1109/iedm19573.2019.8993536](https://doi.org/10.1109/iedm19573.2019.8993536).
- [27] L. Nela et al., "High-performance enhancement-mode AlGaIn/GaN multi-channel power transistors," in *Proc. 33rd Int. Symp. Power Semiconductor Devices ICs (ISPSD)*, Nagoya, Japan, May 2021, pp. 143–146, doi: [10.23919/ISPSD50666.2021.9452238](https://doi.org/10.23919/ISPSD50666.2021.9452238).